



Article

Intraplate thrust orogeny of the Altai Mountains revealed by deep seismic reflection

Lei Zhang^a, Lianfeng Zhao^{a,*}, Liang Zhao^{b,*}, Xiaobi Xie^c, Xiaobo Tian^b, Wenjiao Xiao^{b,d}, Zhenxing Yao^a

^a Key Laboratory of Earth and Planetary Physics, Institute of Geology and Geophysics, Chinese Academy of Sciences, Beijing 100029, China

^b State Key Laboratory of Lithospheric Evolution, Institute of Geology and Geophysics, Chinese Academy of Sciences, Beijing 100029, China

^c Institute of Geophysics and Planetary Physics, University of California at Santa Cruz, CA 95064, USA

^d Xinjiang Institute of Ecology and Geography, Chinese Academy of Sciences, Urumqi 830011, China

ARTICLE INFO

Article history:

Received 1 September 2023

Received in revised form 11 February 2024

Accepted 13 February 2024

Available online 5 March 2024

Keywords:

Altai mountains

Deep seismic reflection profile

Subduction-accretion process

Intraplate deformation pattern

ABSTRACT

The Altai orogen is a typical intracontinental orogen in Central Asia that experienced far-field deformation associated with Indian-Eurasian plate convergence. This region is characterized by uplift comparable to that of the Tianshan Mountains but has a distinct strain rate. Half of the Indo-Asia strain is accommodated by the Tianshan Mountains, whereas the Altai Mountains accommodates only 10%. To elucidate how the Altai Mountains produced such a large amount of uplift with only one-fifth of the strain rate of the Tianshan Mountains, we constructed a detailed crustal image of the Altai Mountains based on a new 166.8-km deep seismic reflection profile. The prestack migration images reveal an antiform within the Erqis crust, an ~10 km Moho offset between the Altai arc and the East Junggar area, and a major south-dipping (30° dip) thrust in the lower crust beneath the Altai Mountains, which is connected to the Moho offset. The south-dipping thrust not only records the southward subduction of the Ob-Zaisan Ocean in the Paleozoic but also controlled the Altai deformation pattern in the Cenozoic with the Erqis antiform. The Erqis antiform prevented the extension of deformation to the Junggar crust. The south-dipping thrust in the lower crust of the Altai area caused extrusion of the lower crust, generating uplift at the surface, thickening of the crust, and steep (~10 km) Moho deepening in the Altai Mountains. This process significantly widened the deformation zone of the Altai Mountains. These findings provide a new geodynamic model for describing how inherited crustal structure controls intraplate deformation without strong horizontal stress.

© 2024 Science China Press. Published by Elsevier B.V. and Science China Press. All rights reserved.

1. Introduction

According to plate tectonics theory, orogenic settings are usually associated with plate boundaries and their immediate vicinity, resulting from interactions between rigid lithospheric plates [1]. However, in the last 50 years, with advances in plate tectonic research, it has been widely accepted that major deformations are not exclusive to plate boundaries but can also occur within plate interiors [2]. In the absence of local plate margin interactions, the deformation must be controlled either by the transmission of horizontal far-field stress from a plate boundary or vertical intraplate stresses via processes such as viscous dripping and delamination or interactions between large igneous provinces at the surface [2,3].

* Corresponding authors.

E-mail addresses: zhaolf@mail.iggcas.ac.cn (L. Zhao), zhaoliang@mail.iggcas.ac.cn (L. Zhao).

Central Asia provides a unique opportunity to study intraplate deformation because intraplate deformation is spread across a broad area in this region, leading to the generation of two typical orogens with intraplate deformation: the Tianshan Mountains and the Altai Mountains (Fig. 1). Many studies have attributed the Cenozoic deformation in Central Asia to the far-field stress transmission resulting from the collision between the Indian and Eurasia plates [7,8]. However, if only the transmission of horizontal stress is considered, it is difficult to explain the almost equivalent amount of deformation between the Tianshan and Altai Mountains. GPS observations suggested that ~20 mm/a (approximately half of the Indo-Asia strain) was accommodated by the Tianshan Mountains, while ~4 mm/a (~10% of the Indo-Asia strain) appeared to be taken up across the Altai Mountains [9,10]. Additionally, there is no seismic or geological evidence, such as lithospheric delamination or a mantle plume, for the generation of vertical stress in the Altai Mountains. Moreover, the Altai Mountains are characterized by transpressional deformation, which can result from the

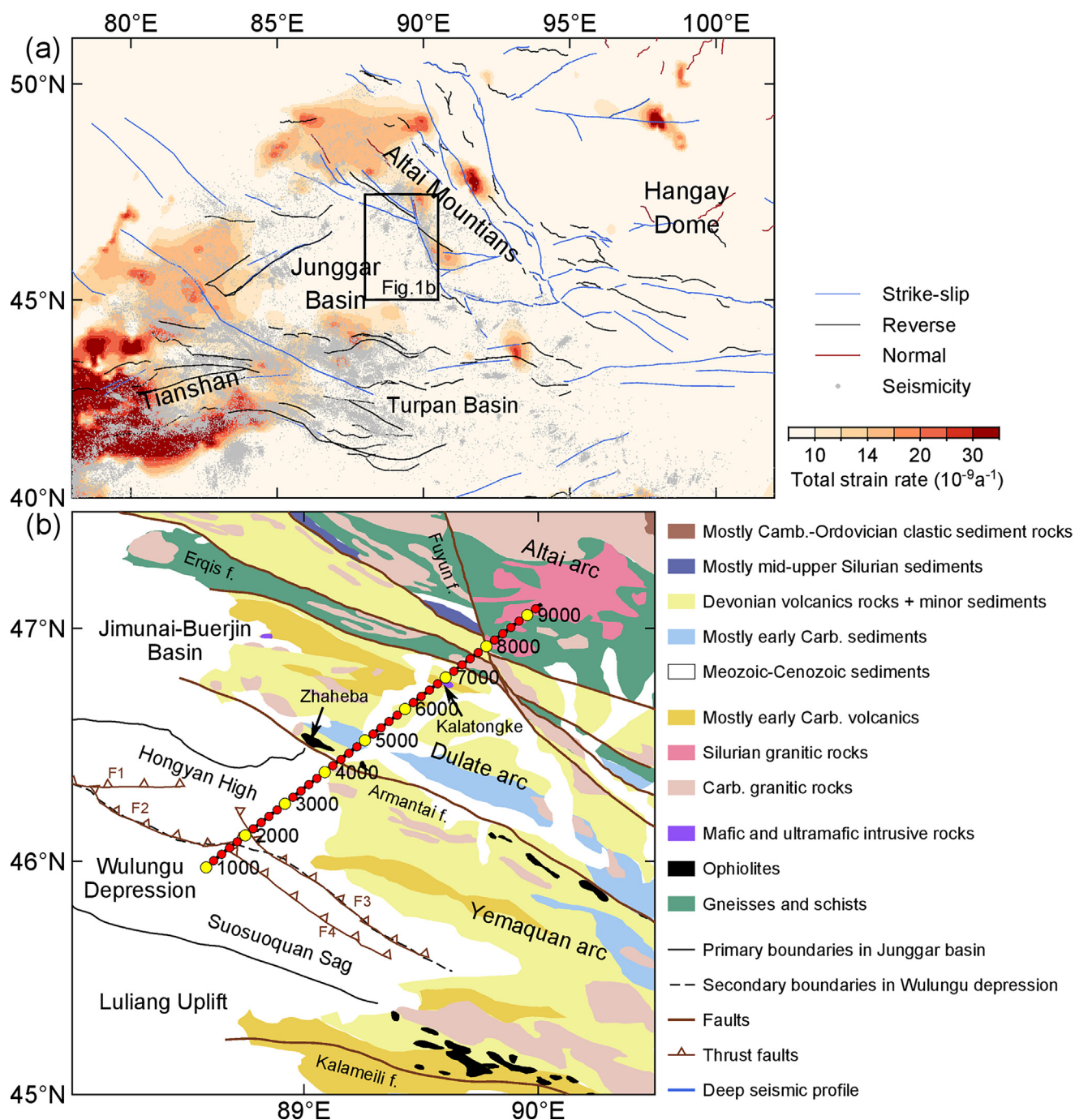


Fig. 1. Regional geology of the Altai Mountains. (a) The total strain rate in and around the Altai Mountains was modified after Kreemer et al. [4]. The colored lines overlaid on the map are faults. The gray circles are earthquakes larger than ML1.0 recorded between 2007 and 2022 (downloaded from the China Earthquake Networks Center). (b) A simplified tectonic map extending from the Junggar Basin to the Chinese Altai terrane is modified from Xiao et al. [5] and Li et al. [6], with its location indicated by a rectangle in Fig. 1a. The blue line represents the reflection seismic profile, in which every 200 common depth points (CDPs) are represented by a filled circle (yellow with label or red). F1, F2, F3, and F4 are thrust faults in the upper crust imaged by seismic data [6].

reactivation of Paleozoic inherited transpressional and/or transtensional strike-slip faults such as the Erqis fault zone [11,12]. Therefore, to resolve the contradiction between the deformation amount and the local stress in the Altai Mountains, it is necessary to consider the role of inherited crustal structures in deformation, as such structures record the tectonic history and the effects of the dynamic process of lithospheric deformation [13,14].

Deep seismic reflection profile is a reliable and robust seismic imaging technique that has been used and improved since the

1970s; this technique provides high-resolution images of the internal structures and physical properties of the crust and uppermost lithosphere [15–17]. In this study, we acquire a 166.8 km-long deep seismic reflection profile that samples the Junggar Basin, East Junggar, and the Chinese Altai Mountains and crosses the Erqis fault in the southwestern margin of the Altai Mountains. With these data, combined with other geophysical and geological data, we first analyze the crustal structures in the Altai-East Junggar region and then elucidate the Paleozoic tectonic activity recorded

by the crustal structures; finally, we discuss how the inherited crustal structures controlled the intraplate deformation process in the Cenozoic.

2. Geological setting

The deep seismic reflection profile investigated in this study is located in the southeastern margin of the Altai Mountains. It extends from the Junggar Basin across the East Junggar terrane and ends in the Chinese Altai Mountains. This belt is a key corridor for understanding the evolution of the Central Asian Orogenic Belt, which is the largest accretionary collage in the world and was formed by the subduction and accretion of juvenile material between the Neoproterozoic and the Paleozoic [18,19]. From SW to NE, the major terranes include the Kalameili ophiolite belt, the Yemaquan arc, the Armantai ophiolite belt, the Dulate arc, the Erqis fault zone, and the Chinese Altai Mountains (Fig. 1b). The Junggar Basin, which is mostly covered by Mesozoic–Cenozoic sediments, is a collage of arcs, accretionary complexes, and trapped oceanic crust that formed in the Paleozoic [5]. The study region contains mainly the Jimunai-Buerjin Basin, the Wulungu Depression, and the Luliang Uplift. The Wulungu Depression can be further divided into the Hongyan High and Suosuoquan Sag based on several thrust faults in the upper crust imaged by seismic data [6]. The East Junggar area and Chinese Altai Mountains have complex Paleozoic tectonic histories [11,19–22]. Based on volcanic–sedimentary strata data, the East Junggar arc is a magmatic arc created by slab-flux melting during subduction in the Devonian–early Carboniferous [23]. It contains two volcanic arcs, one with the Dulate arc in the north and one with the Yemaquan arc in the south. In the late Carboniferous, granitoids in East Junggar were characterized by a transition from I-type granites to A-type granites, suggesting that the tectonic setting shifted from subduction to a postcollisional environment [24,25]. The Erqis fault zone features an E–W-striking crustal-scale thrust, with a length of more than 1000 km and a width of 10–15 km. The kinematics of the Erqis fault and the widespread shear zone-related Au deposits indicate that it was active in the Permian [11,26]. The Chinese Altai Mountains, which are composed of variably deformed and metamorphosed sediments, volcanic rocks, and granitic intrusions, were generated by continental margin activation, reshaping, back-arc oceanic basin formation, and final closure between ~460 and ~408 Ma [27]. Widespread mantle-derived felsic intrusions in the Chinese Altai formed by ridge subduction in the Devonian and postcollisional extension in the late Carboniferous to early Permian [22]. Apatite fission track (AFT) data show that the Altai Mountains were tectonically reactivated in the Mesozoic, coincident with the final closure of the Mongol–Okhotsk Ocean, and were affected by the India–Eurasia collision in the late Cenozoic [28]. Between the late Cretaceous and Paleogene, the Altai Mountains were tectonically quiescent and underwent peneplanation [12]. The almost complete geological records, excellent exposure of ophiolites, magmatic arcs, and accretionary wedges, together with the subsequent collisional orogeny, make this region an ideal natural laboratory for studying the interrelationships between subduction-accretion processes in the Paleozoic and intraplate deformation in the Cenozoic [21,26].

3. Data acquisition and processing

Seismic data were acquired as conventional two-dimensional vertical component explosive-source land profiles. In total, we detonated 715 explosions, including 701 small and medium shots, 11 large shots, and 3 very large shots, from September 6 to October 10, 2018. The data acquisition parameters are listed in Table S1

online. For each shot, the receiver array had a near offset of 20 m and a nominal far offset of 19 km. For some southern shots, restricted by wildlife reserving regulations, 38 km long offsets were used for small and medium shots, 60 km long offsets were used for large shots, and up to 84 km long offsets were used for very large shots. In practice, the far offsets were also dependent on the crooked-line geometry of the recording route. A common receiver interval of 40 m was used for all shots.

The seismic reflection profile was processed using the CGG Geocluster (now Geovation) and Psg-mig seismic processing packages. An industrial reflection processing workflow, including static correction, noise attenuation, amplitude compensation, surface-consistent deconvolution, velocity analysis, residual static corrections, and dip moveout stacking, was applied to generate the stacking image and the Kirchhoff prestack time migration image (Fig. S1 online).

4. Results

Fig. 2a shows a common shot gathered from a 2-ton charge near the center of the survey line. These profiles delineate lateral variations in the crust corresponding to the Junggar Basin, East Junggar arc, and Altai Mountains. Fig. 3b shows a high-quality migrated prestack time migration image from the deep seismic reflection profile. Fig. 3c shows the low-frequency filtered stacking image, which outlines the overall pattern of the underground structures (refer to Fig. S2 online for a comparison between the unfiltered and filtered stack images). The terrane divisions are based on crustal characteristics.

4.1. Moho dislocation between the East Junggar arc and the Altai Mountains

Normally, the Moho discontinuity is defined as a sharp velocity difference between the crust and upper mantle [30]. However, recent studies have revealed that the Moho discontinuity is not always a sharp interface; rather, there are substantial variations in its characteristics both horizontally and vertically globally, particularly in dynamically complex regions [31]. According to deep-reflection seismic profiles, Moho reflections can vary from simple impulse-like signals to a series of multiple arrivals, and some complex regions even lack clear Moho reflection phases [32–34]. The resulting images along the Junggar Basin, the East Junggar arc, and the Chinese Altai Mountains reveal that the Moho discontinuity varies significantly along the profile in terms of both its reflectivity and depth (Fig. 3).

The Moho discontinuity along the profile can be divided into three segments, which are consistent with those of the Junggar Basin, the East Junggar arc, and the Chinese Altai Mountains. The most prominent Moho discontinuity lies beneath the Junggar Basin, where the Moho reflections exhibit large amplitudes at approximately 15 s and continually extend horizontally for approximately 40 km between CDPs 1001 and 3001. Based on the 6.5 km/s average crustal velocity, the crustal thickness reaches ~49 km [29]. The East Junggar Moho reflections are weaker and more diffused and appear as a group of arrivals that lasts for approximately 2 s and extend for approximately 56 km from CDPs 3001 to 5801. For convenience, we took the bottom of these diffusive Moho reflections as the Moho depth. Considering the latest reflections that arrive at ~16 s, we calculated that the East Junggar crust is approximately 52 km thick. The Moho discontinuity beneath the Chinese Altai Mountains is characterized by a series of relatively high-amplitude, laterally discontinuous, south-dipping seismic events. The Moho depth in this section changes from 61.75 km (~19 s) at CDP 6101 to approximately

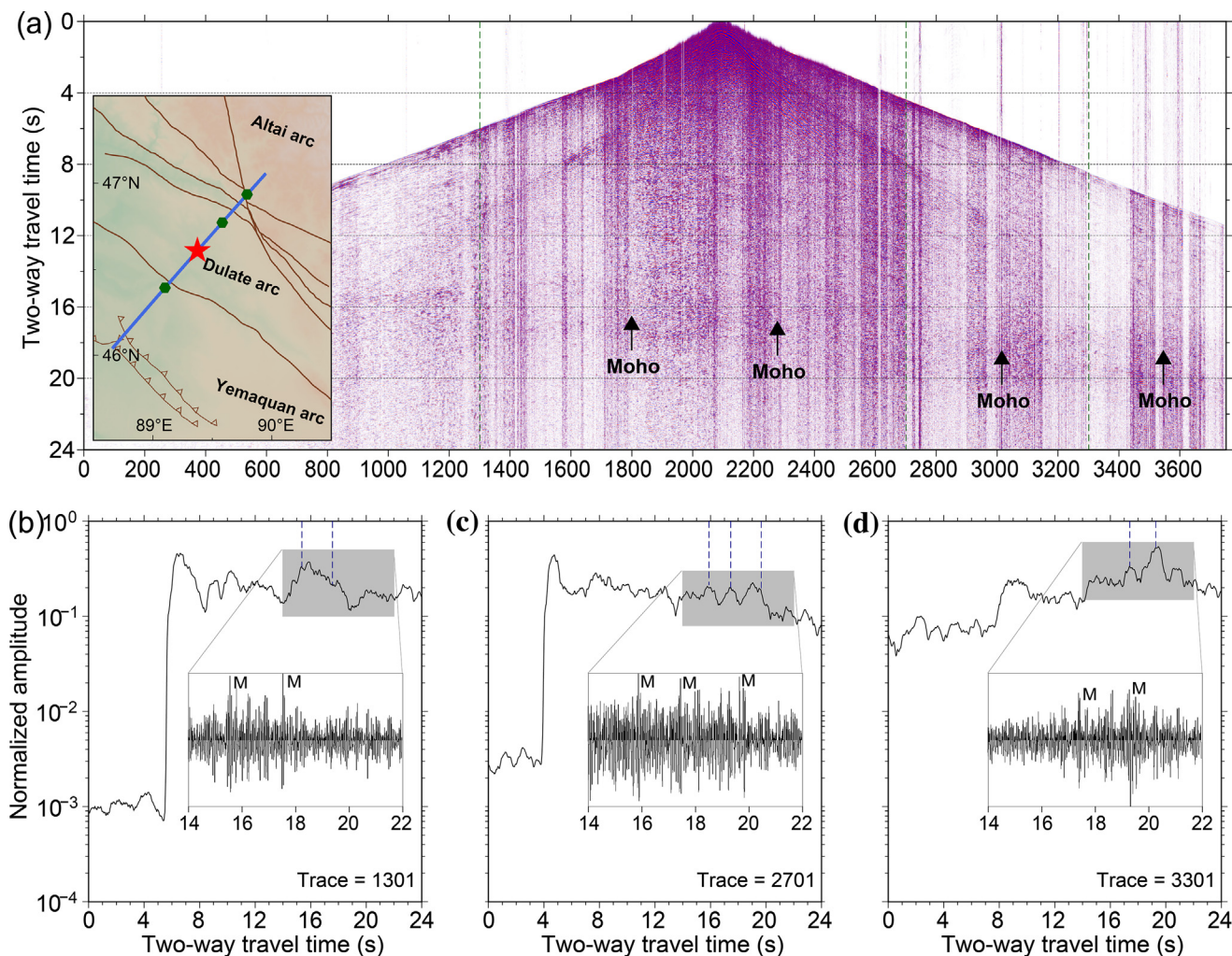


Fig. 2. (a) A typical common shot gather from a 3-ton charge. The interval of each trace is 40 m. The inset map illustrates the locations of the source (red star), receivers (blue line), and three selected traces (green hexagons), overlaid by faults (brown lines). (b–d) The amplitude curves for three selected traces. The related seismograms in the shaded areas are enlarged and shown in the inset map. (b) Trace 1301 from East Junggar arc, where the Moho transition is between ~15 and 17 s. (c) Trace 2701 next to the Kalatongke ore field, where the Moho reflections occur between ~16 and ~20 s. (d) Trace 3301 in the Chinese Altai Mountains, where the Moho transition is between ~17 and ~19 s.

58.5 km (~18 s) at the northern end of the profile. The shallower Moho discontinuities beneath the Junggar Basin and East Junggar arc and the deeper Moho beneath the Altai Mountains are consistent with those of a previous seismic refraction study in the same region [29]. The change in the Moho depth from 16 to 19 s (equivalent to a depth change of approximately 10 km) occurs within a horizontal distance of approximately 6 km between CDPs 5800 and 6100. This change in Moho depth is prominent and can be observed even in a single shot, suggesting the presence of a deep suture between the East Junggar arc and the Altai Mountains (Fig. 2).

4.2. Fine intracrustal structures

Along the reflection profile, the intracrustal reflections can be divided into three domains from south to north (Fig. 3). Zone I corresponds to the Junggar Basin and is characterized by strong reflections throughout the crust. These layers can be further divided into two layers. The upper layer ranges from 0 to 5 s and features randomly oriented reflections with poor continuity, and the lower layer ranges from 5 to 15 s and features gently dipping reflection fabrics with better continuity. An unusually strongly reflective

zone S1 occurs at 14 to 17 s and CDPs 2600 to 3600 (labeled in Fig. 4c). Zone II corresponds to the East Junggar arc, which features clear positive magnetic anomalies, similar to the other Paleozoic magmatic arcs in the Junggar Basin [37]. The lithofacies can also be divided into a strongly reflective upper layer ranging from 0 to 4 s and a “sandwich-like” lower layer ranging from 5 to 15 s. In the shallow part (<2 s) between CDPs 5000 and 5600, a sequence of subhorizontal, high-amplitude reflections are evident and correspond to the surface sediments in the East Junggar arc. The lower layer is composed of several weak scattered patches isolated by zones with layering structures. The weakly reflective zones form three vertical bands labeled W1, W2, and W3 (Fig. 4c). W1 extends from CDPs 4300 to 5000 and corresponds to the Armantai fault on the surface. Taking the Armantai fault as a boundary, its left and right sides feature a series of parallel reflectors but dip in opposite directions. W2 extends from CDPs 5800 to 6400, and W3 extends from CDPs 6700 to 7100. The region between W2 and W3 has no continuous reflectors, but the reflected energy is stronger than that in W2 and W3. Zone III corresponds to the Altai Mountains and features different reflection patterns. In the shallow part (<4 s) between CDPs 7500 and 8300, the reflection reveals a stratified pattern, which may imply a north-dipping thrust nappe. The

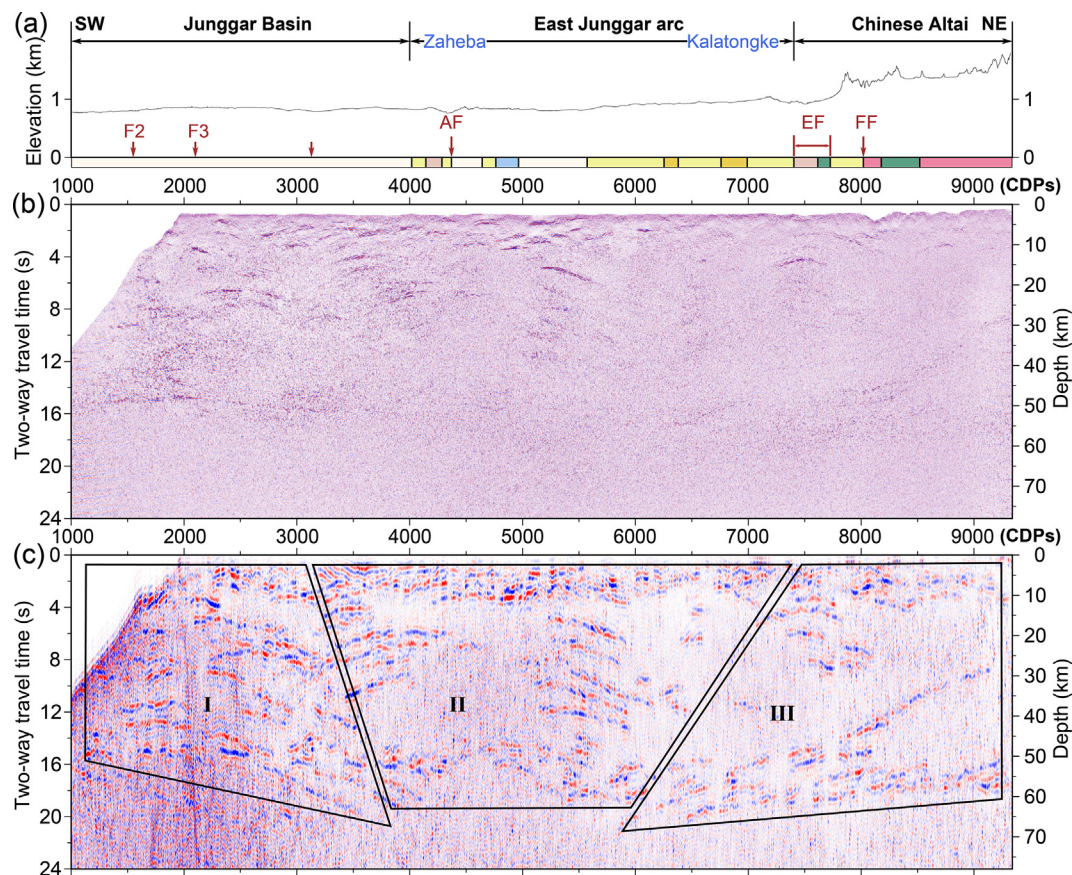


Fig. 3. (a) The elevation and simplified stratigraphy of the area sampled by the seismic profile (the legend is the same as that shown in Fig. 1). AF: Armantai fault. EF: Erqis fault. FF: Fuyun fault. (b) The Kirchhoff prestack time migration profile. (c) Stacking profile after 0.5–2.0 Hz bandpass filtering. In (b–c), the vertical axis on the left is the two-way travel time, and on the right is the approximate depth converted from the travel time by assuming an average crustal velocity of 6.5 km/s [29]. Zones I, II, and III correspond to the Junggar Basin, East Junggar arc, and Altai Mountains, respectively.

reflectivity is generally weak in the central crust except in the ~10 km-wide (from CDPs 7250 to 7750) antiform fold beneath the Erqis fault zone, which ranges from 4 to 10 s, where the reflectivity is strong. In the lower crust, there is a series of reflectors from CDPs 6250 to 9340, which forms a roof-like detached layer. Moving northward, the vertical distance between the detached layer and the Moho discontinuity varies from ~5 to ~30 km.

5. Discussion

5.1. Tectonic events recorded in crustal structures

A series of parallel seismic reflectors were observed in the crust beneath the Wulungu Depression, which is on the northeastern margin of the Junggar Basin (blue lines from CDPs 1500 to 3500 in Fig. 4c). The parallel seismic reflectors can be interpreted as layered sequences or diffractions due to strong velocity anomalies and sharp discontinuities. As migration can greatly suppress the diffractions and the parallel seismic reflectors are still evident in the migration image (Fig. 3b and c), we interpret these parallel seismic reflectors as layered sequences that are signatures of inclined sills. Multiple groups of inclined sills with different inclinations suggest that the Wulungu arc is a collage of several blocks. We interpret this structure as continental crust rather than remnant oceanic crust because the former has often been visualized as a simple, laterally homogeneous, vertically layered pile of mafic rocks that forms at mid-ocean ridges [38]. Several north-dipping

thrusts that can also be observed between the strata have different inclinations and are probably related to the Wulungudong and Lunnan faults that separate the Hongyan High and Suosuoquan Sag at the surface. This structure is consistent with southward-diverging thrust faults in the shallow crust revealed by previous seismic data [6]. Furthermore, borehole data indicate that the Hongyan High underwent significant uplift and exhumation during the late Carboniferous to Permian; it has been buried since the Early Triassic due to subsidence [6]. Therefore, the crustal structure of the Junggar Basin may record tectonic activity in the late Paleozoic. The strongly reflective zone S1 between the Junggar Basin and East Junggar arc results in the deepening of the Moho discontinuity and corresponds to an increase in the local high Bouguer gravity anomaly (~50 mGal, H1 in Fig. 4a). Therefore, we infer that S1 is a high-density body that may have resulted from the collision between the Wulungu arc and East Junggar arc.

The crustal structure of the East Junggar arc is characterized by three narrow, vertical, weak reflective zones in the deep crust and an asymmetric fault system in the upper crust centered on the Armantai fault (from CDPs 3000 to 7100 in Fig. 4c). Generally, a lack of reflectivity or very weak reflections indicates that the structure is too fine or that the velocity contrasts are too weak to be detected by seismic signals [16]. The lack of heterogeneities capable of back-scattering seismic energy that results in a reflection fabric suggests that the area has been homogenized. This could be the result of magma injection or metamorphism. W1 connects to the asymmetric fault system in the upper crust centered on the Armantai fault, which separates the Yemaquan and Dulate arcs

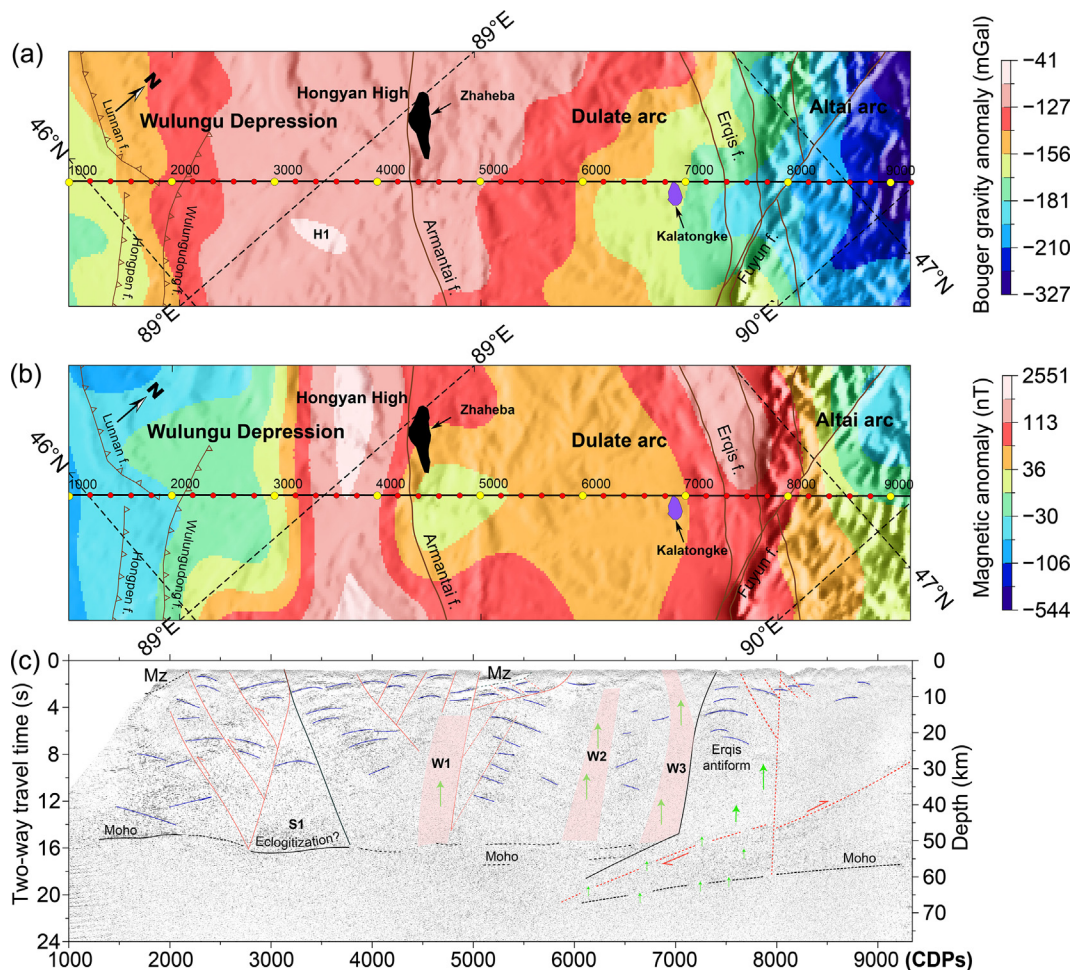


Fig. 4. (a) Simple Bouguer gravity anomalies along the profile overlain by faults, the Zhaheba ophiolite, and the Kalatongke mafic rocks. The Bouguer gravity anomaly data are from the International Center for Global Earth Models (ICGEM) with the Earth Global Model 08 (EGM08) available at a spatial resolution of 2.5×2.5 arc-minutes [35]. (b) The magnetic anomaly data along the profile are from the Earth Magnetic Anomaly Grid, which are available at a spatial resolution of 2×2 arc-minutes (EMAG2) [36]. (c) The seismic reflection interpretation includes block boundaries (black lines), faults (red lines), strata (blue lines), the Moho discontinuity (dotted black lines), and weak reflection zones (W1, W2, and W3).

on the surface. Therefore, W1 marks the crustal boundary that separates the south-dipping strata in the south beneath the Yemaquan arc and the north-dipping strata in the north beneath the Dulate arc. Furthermore, the location of W1 correlates well with the surface of the Zhaheba ophiolite complex (Fig. 4), which mainly consists of ultramafic rocks, gabbro, diorite, basalt and chert intruded by diabase dikes and diorite porphyry and contains lenses of garnet pyroxenite and quartz-magnetite [39]. Supersilicic and supertitanic garnets have been recorded in garnet pyroxenite from the Zhaheba complex, indicating that they underwent ultrahigh-pressure (UHP) metamorphism [40]. Moreover, garnet amphibolite, quartz-magnetite, and Nb-enriched basalt have been reported in the Zhaheba ophiolite mélangé; one interpretation of these observations and geochronological data is that the Zhaheba ophiolite and the UHP metamorphic rocks underwent exhumation in the early Permian [40–42]. Consequently, the formation of W1 was likely the result of episodic metamorphic activity in the Paleozoic. Both W2 and W3 roughly correspond to early Carboniferous volcanic rocks at the surface (Figs. 3 and 4) and are likely indicators of plutons, stocks, and dikes formed by magmatic activity in the early Carboniferous [16,43,44]. However, unlike W2, which is located in the center of the Dulate arc, W3 is adjacent to the Erqis fault zone. The shear zone-related gold deposits and structural and geochronological data in the Erqis shear zone indicate that it

underwent multiphase deformation [26,45]. Furthermore, W3 also corresponds to the Cu-Ni deposit Kalatongke, which intruded during the early Permian [46–48]. Positive ε_{Nd} values (4 to 10) and significant negative Nb anomalies for both intrusive and extrusive rocks in the Kalatongke deposit imply that the metallogenic magma was derived from the depleted mantle and contaminated by juvenile arc crust [47]. Therefore, the formation of W3 may be related to multiple phases of magmatism and shear deformation activities, and W2 may be related to mainly magmatism.

In the Altai crust, a north-dipping thrust nappe can be observed in the upper crust (<4 s between CDPs 7500 and 8300), and a south-dipping detached layer can be observed in the lower crust (~ 20 s at CDP 6250 to ~ 9 s at CDP 9340). They form a typical crustal-scale crocodile structure oriented in a SW direction (Fig. 4). The weak reflectivity in the middle crust indicates that this area could have been homogenized due to multistage magmatism and metamorphism in the Altai Mountains [6,20,22,27,49,50]. The south-dipping detached layer in the lower crust and the Moho discontinuity form a strong reflective wedge that widens northward and intrudes southward. Although the reflectivity is strong in the wedge, the continuity of the reflectors is poor. A series of small weak reflective zones penetrate the strong reflectors (at 12–20 s between CDPs 6250 and 9340 in Fig. 3c), indicating that the formation of the south-dipping wedge occurred before that of the weak

reflective zones, which may be related to the most recent magmatism and shear deformation in the early Permian [26,45,47,48]. The wedge intrudes into the mantle of the East Junggar arc at approximately CDP 6000 and results in an ~3 s Moho offset. The regional thickening of the Chinese Altai crust also corresponds to the decrease in Bouguer gravity anomalies (Fig. 4a).

5.2. Southward subduction of the Ob-Zaisan Ocean in the Paleozoic

The Altai-Junggar area is widely accepted to be characterized by multiple Paleozoic subduction-accretion systems [21,22,51]. In the early Paleozoic, this region was composed of arcs and oceans such as the Altai, Dulate, Wulungu, and Yemaquan arcs, the Ob-Zaisan Ocean, and branches of the Junggar Ocean (Fig. 5). With the closure of oceans, island arcs underwent multiple episodes of subduction, collision, and accretion, all of which contributed to the amalgamation of island arcs and accretionary complexes. Generally, an intracrustal structure can record such a tectonic evolution, but this capability is often disturbed by the most recent or strongest tectonic activity, making it difficult to correctly determine temporal changes without including other observations. The crust beneath the Wulungu arc is strongly reflective and characterized by a series of thrust faults. Based on shallow seismic reflection data, the Wulungu Depression can be subdivided into two NW-trending tectonic units, the Suosuoquan Sag and the Hongyan High, separated by south-verging thrust faults [6]. The divergent thrust faults correspond well to the intracrustal thrust system observed in our profile. Furthermore, based on borehole stratigraphic data, southward thrust activity can be constrained to the lower Carboniferous and Permian, which has caused distinct uplift and exhumation of the Hongyan High [6]. The crust of the East Junggar arc is characterized by several extensional imprints, including an asymmetric sedimentary layer and strata separated by weak reflection zones. These extensional imprints are consistent with the presence of widespread A-type granites in this area, which indicates postcollisional extension [48,53]. Combined with the geochronology of granitoids in this area, it is possible to date the most recent period of postcollisional extensional activity, which was accompanied by

strong magmatism and metamorphism, to between the late Carboniferous and the Permian [24,25,50].

The south-dipping thrust in the lower crust of the Altai Mountains provides a valuable proxy for the subduction polarity of the Ob-Zaisan Ocean [24]. Previous studies supported north-dipping subduction beneath the Altai Mountains, as the rock units of the Altai Mountains exhibit southward younging [21,54]. However, the crustal structure of the Altai arc has no imprint on northward subduction, and the south-dipping thrust even contradicts this interpretation. Because the south-dipping thrust was cut off by a series of zones with weak reflectivity (Fig. 3), the south-dipping thrust should have formed before the weak reflective zones. The zones with weak reflectivity may have been caused by small-scale magma upwelling or by the strike-slip motion of fragments perpendicular to the profile. The most recent magmatism in this area recorded by granitoids was in the early Permian [47,48]. Mafic rocks in the Kalatongke deposit have positive ϵ_{Nd} values and primitive mantle-normalized trace element patterns enriched in large ion lithophile elements (LILEs), indicating that mantle-derived basaltic magmatism might have occurred in the early Permian [47,55]. Accordingly, this was the most likely mechanism for the formation of the weakly reflective zones. The strike-slip motion of fragments perpendicular to the profile cannot be excluded. However, the latest strike-slip motion in this region also occurred in the early Permian based on kinematic data and the geochronology of shear zone-related Au deposits [26,45]. Hence, we can confirm that the weakly reflective zones formed during the early Permian and that the south-dipping thrust formed before the early Permian. The formation of the south-dipping thrust in the Paleozoic strata indicates the south-dipping subduction of the Ob-Zaisan Ocean. A recent report about geochronological, geochemical, and isotopic data for the magmatic rocks collected from the northern part of the Dulate arc suggested that there was mid-oceanic ridge subduction during the latest Carboniferous to Permian [56]. With this finding, combined with previous reports of boninites, Nb-enriched basalts, and adakites that imply a forearc setting for the northern part of the Dulate arc in the Devonian [57,58], it can be concluded that the mid-oceanic ridge of the Ob-Zaisan Ocean subducted southward beneath the Dulate arc

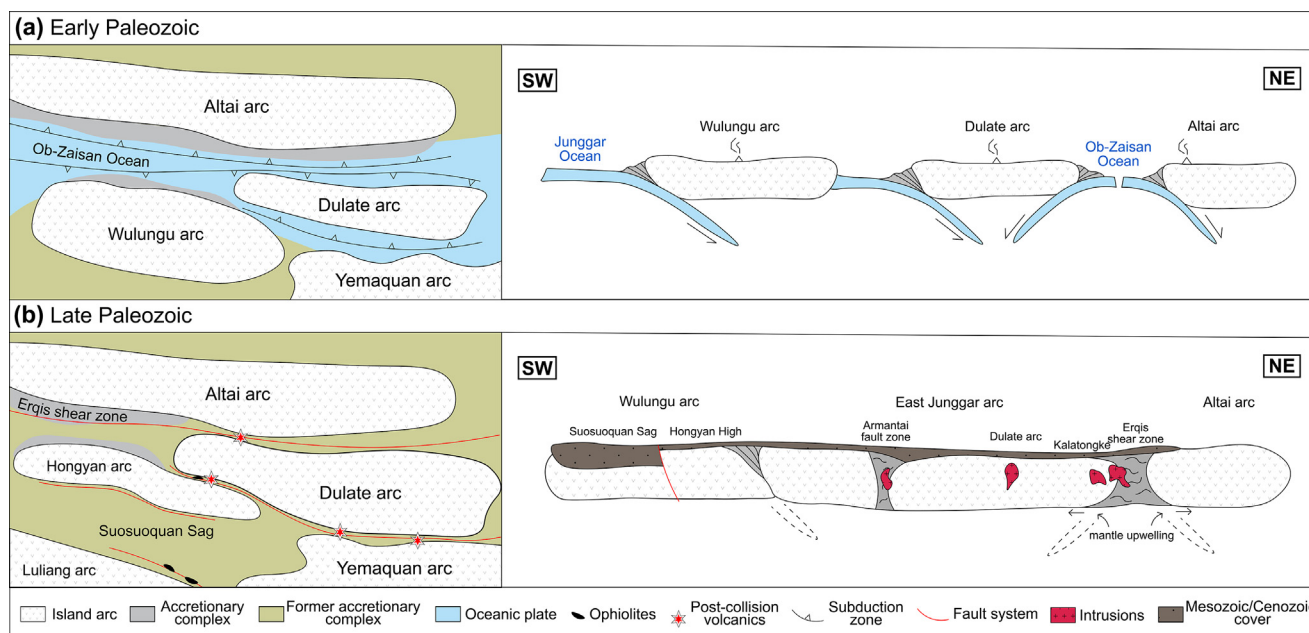


Fig. 5. Cartoons illustrating the tectonic evolution of the Altai-East Junggar area during the Paleozoic (modified after Refs. [6,22,52]). (a) During the early Paleozoic; (b) during the late Paleozoic.

during the latest Carboniferous to Permian [56]. Therefore, the geological record was used to confirm that the Ob-Zaisan Ocean underwent southward subduction in the Paleozoic in addition to north-dipping subduction.

5.3. Cenozoic intraplate deformation controlled by the Erqis antiform and south-dipping low-angle detachment layer

In addition to recording the southward subduction of the Ob-Zaisan Ocean in the Paleozoic, the south-dipping thrust in the lower crust of the Altai Mountains strongly influenced its deformation pattern in the Cenozoic. Previous studies have long emphasized the important role of lithospheric inheritance in intraplate deformation, but the type of inherited structure and its role in intraplate deformation are still controversial. For example, the crustal deformation of the Ouachita orogen in the southeastern United States was driven by mantle scarring [3]. Receiver function images of the Tianshan crustal structure were used to demonstrate that the inherited rheological heterogeneities controlled shallow brittle deformation [10]. The seismic reflection profile presented here provides a new example of an inherited lower crustal thrust that controlled intraplate deformation.

The Altai Mountains have undergone multiphase tectonic activities, including accretion-collision events in the Paleozoic and reactivation in the Cenozoic. However, whether accretion-collision events in the Paleozoic generated a large mountain belt in the Altai is unclear. However, an apatite fission track (APT) analysis revealed that the Altai region was reduced to an area of low relief between ~ 75 and ~ 25 – 20 Ma after a period of tectonic quiescence and peneplanation [59]. This is supported by sediments in the Junggar Basin, which experienced almost no subsidence throughout that time [59]. Therefore, the current topography of the Altai Mountains was mainly the result of tectonic reactivation in the late Cenozoic [12,60]. APT thermochronological data indicate that the intraplate deformation of the Altai Mountains commenced at ~ 5 Ma [12]. Most studies have attributed the Cenozoic deformation of the Altai Mountains to the far-field effects of the collision between the Indian and Eurasia plates [7,8]. Recent geodynamic modeling has supported this causation, indicating that the rigid

India, Tarim and Junggar blocks effectively transmitted plate-convergent stress from the Tibetan Plateau to the Asian interior [61]. However, on the northeastern margin of the deformation zone, it is difficult to explain the wide and evident topography of the Altai Mountains by stress transmission alone.

The crustal structure of the Altai Mountains reveals a new orogenic mechanism, driven by a low-angle detachment thrust, to explain the contradiction between weak strain and a wide deformation zone. The most prominent feature of this profile is the Moho offset between the Altai Mountains and the East Junggar arc. The Moho offset can reach ~ 9.75 km if an average crustal velocity of 6.5 km/s is assumed [29]. The Moho offset in the Altai Mountains is connected to an intracrustal thrust with an $\sim 30^\circ$ dip angle. This deep Moho offset is located nearly 30 km south of the Erqis fault zone and is the surface trace of the southeastern margin of the Altai Mountains. Beneath the Erqis fault zone, there is a crustal antiform. Based on our seismic reflection interpretation and the above analysis, we propose a new model for the crustal deformation of the Altai Mountains (Fig. 6). The inherited low-angle thrust in the lower crust of the Altai Mountains accommodated the far-field horizontal stress, which caused the thrusting of the upper and middle crust and extrusion of the lower crust. The Erqis antiform in the southwestern margin of the Altai Mountains absorbed the deformation and prevented strong deformation of the Junggar crust. This can be further confirmed by the decreasing strain rate and seismicity from the Erqis fault to East Junggar (Fig. S3 online). This deformation caused the uplift of the Altai Mountains, forming a steep front along the Erqis fault zone and gradually decreasing deformation in the Altai Mountains from south to north (Fig. S3 online). Moreover, the Altai lower crust escaped along the thrust and deepened the Moho beneath the Altai range. The decrease in the Bouguer gravity anomaly from the East Junggar area to the Altai range is consistent with the change in Moho depth, which provides additional evidence for our deformation model (Fig. 4).

Our deformation model demonstrates that the inherited structure in the crust controlled intraplate deformation when the stress was relatively weak. The low-angle thrust in the Altai lower crust significantly widened the deformation zone. These findings

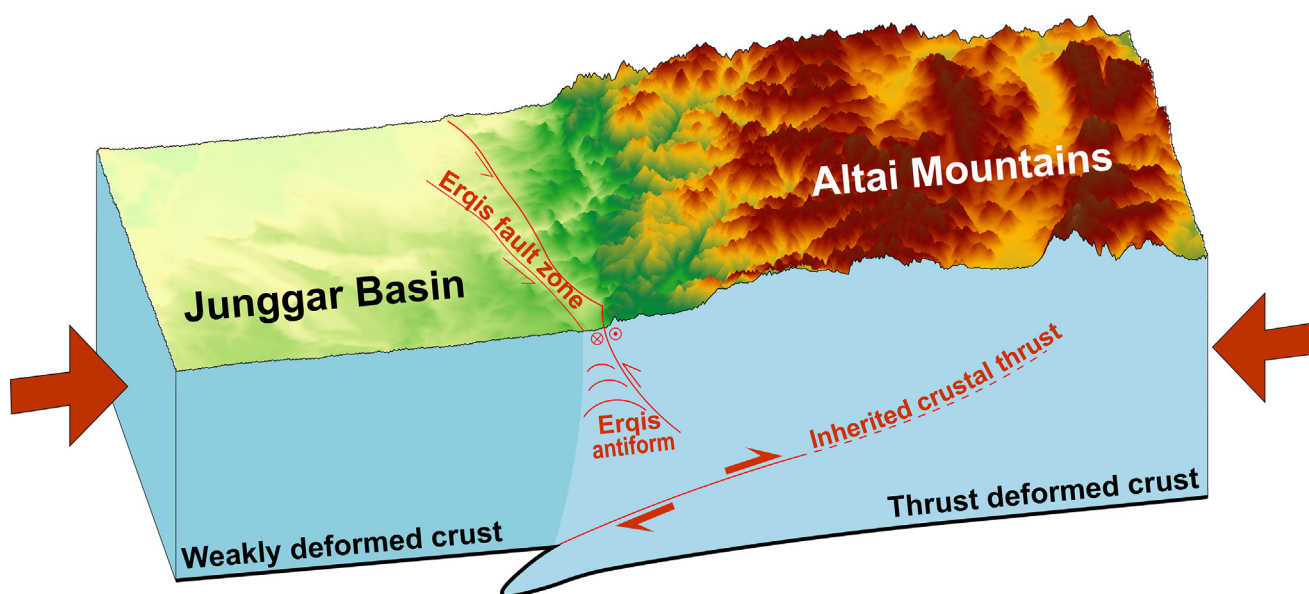


Fig. 6. Cartoon of the residual crustal detachment layer accommodating convergence between the Junggar Basin and Altai Mountains. On the surface, the thin red curves represent the Erqis fault zone. In the cross-section, the bold black lines are the Moho constrained by the reflection profile; the red lines mark strong reflective layers in the Altai crust.

provide a robust and testifiable rejuvenation model for the Altai Mountains and have promising implications for intraplate deformation worldwide.

6. Conclusions

We performed data acquisition and migration imaging for a 166.8 km-long deep seismic reflection profile in the southwestern margin of the Altai Mountains in central Asia. By integrating geological observations with images from the deep seismic reflection profile, we obtained the following results: (1) We discovered the distinct architectures of the crust and uppermost mantle beneath the Junggar Basin, East Junggar arc, and Altai Mountains. (2) We documented the fine structures of the Junggar Basin crust, including layers and faults at multiple scales, which formed during the accretion of allochthonous continental landmass rather than remnant oceanic crust. (3) The Erqis fault zone, which separates the East Junggar arc from the Altai Mountains, contains a major crustal antiform, which very likely absorbed compression in the Cenozoic. (4) The south-dipping ductile shear zone in the lower crust of the Altai Mountains contributed to an ~10 km offset of the Moho between the East Junggar and Altai Mountains. The south-dipping thrust in the lower crust of the Altai Mountains was formed before the Permian by the southward subduction of the Ob-Zaisan Ocean in the Paleozoic, and it controlled the Cenozoic deformation pattern and formation of the Erqis antiform, leading to the steep mountain front at the Eriqis fault.

Conflict of interest

The authors declare that they have no conflict of interest.

Acknowledgments

This work was supported by the National Key Research and Development Program of China (2017YFC0601206) and the National Natural Science Foundation of China (41974061, 41974054). This is a contribution to IGCP 662. All field data acquisition was completed by the Bureau of Geophysical Prospecting (BGP) INC., China National Petroleum Corporation (CNPC). Industrial data processing was conducted by the Beijing Paitesen Company. Some figures were created using the Generic Mapping Tool (GMT) [62]. We thank Drs. Bo Wan, Xusong Yang, Xingwang Xu at the Institute of Geology and Geophysics, Chinese Academy of Sciences, Dr. Wenhui Li at the Institute of Geology, Chinese Academy of Geological Sciences, and Dr. Youxue Wang at the Guilin University of Technology for their constructive suggestions.

Author contributions

Lianfeng Zhao, Liang Zhao, and Wenjiao Xiao designed and directed this project. Lei Zhang interpreted the data, conceptualized the idea, plotted the figures, and wrote the original manuscript. Lianfeng Zhao, Liang Zhao, Xiaobi Xie, Xiaobo Tian, and Wenjiao Xiao discussed the results and commented on the manuscript. Zhenxin Yao supervised the project. All the authors approved the final version of the manuscript.

Data availability

For the deep seismic reflection profile across the northeastern margin of the Junggar Basin and the Altai Mountains, the stack profiles and the Kirchhoff prestack time migration profiles in both segy and jpg formats can be accessed at the World Data Center

for Geophysics, Beijing, at <http://www.geophys.ac.cn/ArticleDataInfo.asp?MetalId=602> (last accessed Jan 2024).

Appendix A. Supplementary materials

Supplementary materials to this article can be found online at <https://doi.org/10.1016/j.scib.2024.03.011>.

References

- [1] Dewey JF, Bird JM. Mountain belts and the new global tectonics. *J Geophys Res* 1970;75:2625–47.
- [2] Raimondo T, Hand M, Collins WJ. Compressional intracontinental orogens: Ancient and modern perspectives. *Earth Sci Rev* 2014;130:128–53.
- [3] Stephenson R, Egholm DL, Nielsen SB, et al. Role of thermal refraction in localizing intraplate deformation in southeastern Ukraine. *Nat Geosci* 2009;2:290–3.
- [4] Kreemer C, Blewitt G, Klein EC. A geodetic plate motion and global strain rate model. *Geochem Geophys Geosys* 2014;15:3849–89.
- [5] Xiao WJ, Windley BF, Han CM, et al. Late paleozoic to early Triassic multiple roll-back and oroclinal bending of the Mongolia collage in Central Asia. *Earth Sci Rev* 2018;186:94–128.
- [6] Li D, He D, Tang Y. Reconstructing multiple arc-basin systems in the Altai-Junggar area (NW China): Implications for the architecture and evolution of the western central Asian Orogenic Belt. *J Asian Earth Sci* 2016;121:84–107.
- [7] Gregory LC, Mac Niocaill C, Walker RT, et al. Vertical axis rotation (or lack thereof) of the eastern Mongolian Altay Mountains: Implications for far-field transpressional mountain building. *Tectonophysics* 2018;736:31–46.
- [8] Molnar P, Tapponnier P. Cenozoic tectonics of Asia: Effects of a continental collision. *Science* 1975;189:419–26.
- [9] Calais E, Vergnolle M, San'kov V, et al. GPS measurements of crustal deformation in the Baikal-Mongolia area (1994–2002): Implications for current kinematics of Asia. *J Geophys Res* 2003;108:1481–503.
- [10] Li W, Chen Y, Yuan X, et al. Intracontinental deformation of the Tianshan orogen in response to India-Asia collision. *Nat Commun* 2022;13:3738.
- [11] Briggs SM, Yin A, Manning CE, et al. Late Paleozoic tectonic history of the Ertix fault in the Chinese Altai and its implications for the development of the Central Asian orogenic system. *Geol Soc Am Bull* 2007;119:944–60.
- [12] Buslov MM, Kokh DA, De Grave J. Mesozoic-Cenozoic tectonics and geodynamics of Altai, Tien Shan, and Northern Kazakhstan, from apatite fission-track data. *Russ Geol Geophys* 2008;49:648–54.
- [13] Huangfu P, Li Z-H, Gerya T, et al. Multi-terrane structure controls the contrasting lithospheric evolution beneath the western and central-eastern Tibetan Plateau. *Nat Commun* 2018;9:3780.
- [14] Tian X, Bai Z, Klempner SL, et al. Crustal-scale wedge tectonics at the narrow boundary between the Tibetan Plateau and Ordos block. *Earth Planet Sci Lett* 2021;554:116700.
- [15] Oliver J. Exploration of the continental basement by seismic reflection profiling. *Nature* 1978;275:485–8.
- [16] Drummond B, Lyons P, Goleby B, et al. Constraining models of the tectonic setting of the giant Olympic dam iron oxide-copper-gold deposit, South Australia, using deep seismic reflection data. *Tectonophysics* 2006;420:91–103.
- [17] Gao R, Lu ZW, Klempner SL, et al. Crustal-scale duplexing beneath the Yarlung Zangbo suture in the western Himalaya. *Nat Geosci* 2016;9:555–60.
- [18] Sengor AMC, Natalin BA, Burtman VS. Evolution of the Altaid tectonic collage and Paleozoic crustal growth in Eurasia. *Nature* 1993;364:299–307.
- [19] Xiao WJ, Windley BF, Yuan C, et al. Paleozoic multiple subduction-accretion processes of the southern Altaids. *Am J Sci* 2009;309:221–70.
- [20] Windley BF, Alexeiev D, Xiao WJ, et al. Tectonic models for accretion of the Central Asian Orogenic Belt. *J Geol Soc* 2007;164:31–47.
- [21] Xiao WJ, Han CM, Yuan C, et al. Middle Cambrian to Permian subduction-related accretionary orogenesis of Northern Xinjiang, NW China: Implications for the tectonic evolution of Central Asia. *J Asian Earth Sci* 2008;32:102–17.
- [22] Cai KD, Sun M, Yuan C, et al. Carboniferous mantle-derived felsic intrusion in the Chinese Altai, NW China: Implications for geodynamic change of the accretionary orogenic belt. *Gondwana Res* 2012;22:681–98.
- [23] Zhang Z, Zhou G, Kusky TM, et al. Late Paleozoic volcanic record of the Eastern Junggar terrane, Xinjiang, Northwestern China: Major and trace element characteristics, Sr-Nd isotopic systematics and implications for tectonic evolution. *Gondwana Res* 2009;16:201–15.
- [24] Li PF, Sun M, Rosenbaum G, et al. Late Paleozoic closure of the Ob-Zaisan Ocean along the Irtysh shear zone (NW China): Implications for arc amalgamation and oroclinal bending in the Central Asian orogenic belt. *Geol Soc Am Bull* 2017;129:547–69.
- [25] Liu X, Liu W, Si C. Petrogenesis and source rocks of the high-K calc-alkaline and shoshonitic I-type granitoids in the northwestern part of East Junggar, NW China. *Lithos* 2019;326–327:298–312.
- [26] Wan B, Xiao WJ, Zhang LC, et al. Contrasting styles of mineralization in the Chinese Altai and East Junggar, NW China: Implications for the accretionary history of the southern Altaids. *J Geol Soc* 2011;168:1311–21.
- [27] Wang T, Hong DW, Jahn BM, et al. Timing, petrogenesis, and setting of Paleozoic synorogenic intrusions from the Altai Mountains, Northwest China:

- Implications for the tectonic evolution of an accretionary orogen. *J Geol* 2006;114:735–51.
- [28] De Grave J, Buslov MM, Van den haute P, distant effects of India-Eurasia convergence and Mesozoic intracontinental deformation in Central Asia: Constraints from apatite fission-track thermochronology. *J Asian Earth Sci* 2007;29:188–204.
- [29] Wang YX, Mooney WD, Yuan XC, et al. The crustal structure from the Altai mountains to the Altyn Tagh fault, Northwest China. *J Geophys Res* 2003;108: B62322.
- [30] Mohorovicic A. Godišnje izvješće zagrebačkog meteorološkog opservatorija za godinu 1909. 1910;Godina IX:63.
- [31] Thybo H, Artemieva IM, Kennett B. Moho: 100 years after Andrija Mohorovičić. *Tectonophysics* 2013;609:1–8.
- [32] Chadwick RA, Pharaoh TC. The seismic reflection Moho beneath the United Kingdom and adjacent areas. *Tectonophysics* 1998;299:255–79.
- [33] Cook FA. Fine structure of the continental reflection Moho. *Geol Soc Am Bull* 2002;114:64–79.
- [34] Mooney WD, Meissner R. *Continental Lower Crust*. Amsterdam: Elsevier; 1992. p. 45–79.
- [35] Pavlis NK, Holmes SA, Kenyon SC, et al. The development and evaluation of the Earth Gravitational Model 2008 (EGM2008). *J Geophys Res* 2012;117:B04406.
- [36] Maus S, Barckhausen U, Berkenbosch H, et al. EMAG2: A 2-arc min resolution Earth Magnetic Anomaly Grid compiled from satellite, airborne, and marine magnetic measurements. *Geochem Geophys Geosys* 2009;10:Q08005.
- [37] Yang X, Tian X, Windley BF, et al. The role of multiple trapped oceanic basins in continental growth: Seismic evidence from the southern altaids. *Geophys Res Lett* 2022;49:e2022GL098548.
- [38] De Voogd B, Keen C. *Geophysics*. Boston: Springer; 1990. p. 181–91.
- [39] Zhang P, Yu C, Zeng X. Crustal electrical structure of the Zhaheba complex imaged by magnetotelluric data and its tectonic implications. *Appl Sci* 2021;11:10013.
- [40] Niu H, Zhang H, Shan Q, et al. Discovery of super-silicic and super-titanic garnets in garnet-pyroxenite in Zhaheba and its geological significance. *Chin Sci Bull* 2008;53:2186–91.
- [41] Niu HC, Shan Q, Zhang HX, et al. $^{40}\text{Ar}/^{39}\text{Ar}$ geochronology of the ultrahigh-pressure metamorphic quartz-magnetite in Zaheba, eastern Junggar, Xinjiang. *Acta Petrol Sin* 2007;23:1627–34.
- [42] Niu H, Shan Q, Zhang B, et al. Discovery of garnet amphibolite in Zaheba ophiolitic melange, eastern Junggar, NW China. *Acta Petrol Sin* 2009;25:1484–91.
- [43] Goleby BR, Huston DL, Lyons P, et al. The Tanami deep seismic reflection experiment: An insight into gold mineralization and Paleoproterozoic collision in the North Australian Craton. *Tectonophysics* 2009;472:169–82.
- [44] Lü Q, Yan J, Shi D, et al. Reflection seismic imaging of the Lujiang-Zongyang volcanic basin, Yangtze Metallogenic Belt: An insight into the crustal structure and geodynamics of an ore district. *Tectonophysics* 2013;606:60–77.
- [45] Li PF, Sun M, Rosenbaum G, et al. Structural evolution of the Irtys Shear Zone (northwestern China) and implications for the amalgamation of arc systems in the Central Asian Orogenic Belt. *J Struct Geol* 2015;80:142–56.
- [46] Pirajno F, Mao JW, Zhang ZC, et al. The association of mafic-ultramafic intrusions and A-type magmatism in the Tian Shan and Altay orogens, NW China: Implications for geodynamic evolution and potential for the discovery of new ore deposits. *J Asian Earth Sci* 2008;32:165–83.
- [47] Li C, Zhang M, Fu P, et al. The Kalatongke magmatic Ni-Cu deposits in the Central Asian Orogenic Belt, NW China: Product of slab window magmatism? *Miner Deposita* 2012;47:51–67.
- [48] Zhang ZH, Mao JW, Du AD, et al. Re-Os dating of two Cu-Ni sulfide deposits in northern Xinjiang, NW China and its geological significance. *J Asian Earth Sci* 2008;32:204–17.
- [49] Jiang YD, Schulmann K, Sun M, et al. Structural and geochronological constraints on Devonian suprasubduction tectonic switching and Permian collisional dynamics in the Chinese Altai, Central Asia. *Tectonics* 2019;38:253–80.
- [50] Cai K, Sun M, Yuan C, et al. Geochronology, petrogenesis and tectonic significance of peraluminous granites from the Chinese Altai, NW China. *Lithos* 2011;127:261–81.
- [51] Xiao WJ, Huang BC, Han CM, et al. A review of the western part of the Altaids: A key to understanding the architecture of accretionary orogens. *Gondwana Res* 2010;18:253–73.
- [52] Xiao WJ, Santosh M. The western Central Asian Orogenic Belt: A window to accretionary orogenesis and continental growth. *Gondwana Res* 2014;25:1429–44.
- [53] Han BF, Ji JQ, Song B, et al. SHRIMP zircon U-Pb ages of Kalatongke No. 1 and Huangshandong Cu-Ni-bearing mafic-ultramafic complexes, North Xinjiang, and geological implications. *Chin Sci Bull* 2004;49:2424–9.
- [54] Windley BF, Kroner A, Guo JH, et al. Neoproterozoic to Paleozoic geology of the Altai orogen, NW China: New zircon age data and tectonic evolution. *J Geol* 2002;110:719–37.
- [55] Gao J-F, Zhou M-F. Magma mixing in the genesis of the Kalatongke dioritic intrusion: Implications for the tectonic switch from subduction to post-collision, Chinese Altay, NW China. *Lithos* 2013;162-163:236–50.
- [56] Gan J, Xiao W, Mao Q, et al. A newly defined latest Carboniferous-Permian ridge subduction in the southern Altaids: Insights from adakitic, S-type, and I-type granitoids in the northern East Junggar (NW China). *Int Geol Rev* 2024;66:1634–1662.
- [57] Zhang HX, Niu H, Yu XY, et al. Geochemical characteristics of the Shaerbulake boninites and their tectonic significance, Fuyun County, northern Xinjiang, China. *Geochim* 2003;32:155–60.
- [58] Xu J, Mei H, Yu X, et al. Adakites related to subduction in the northern margin of Junggar arc for the late Paleozoic: Products of slab melting. *Chin Sci Bull* 2001;46:1312–6.
- [59] Yuan W, Carter A, Dong J, et al. Mesozoic-Tertiary exhumation history of the Altai Mountains, northern Xinjiang, China: New constraints from apatite fission track data. *Tectonophysics* 2006;412:183–93.
- [60] Frankel K, Wegmann K. Hanging-wall topographic expression in oblique contractional orogens. *AGU Fall Meeting Abstracts* 2010.
- [61] Huangfu P, Fan W, Li Z-H, et al. Linkage between the India-Asia collision and far-field reactivation of the Altai mountains. *Palaeogeogr Palaeoclimatol Palaeoecol* 2023;616:111478.
- [62] Wessel P, Luis JF, Uieda L, et al. The generic mapping tools version 6. *Geochem Geophys Geosys* 2019;20:5556–64.



Lei Zhang is a Ph.D. graduate from the Institute of Geology and Geophysics, Chinese Academy of Sciences, now works as a Postdoc at Peking University. Her research interest focuses on exploring the crust and upper mantle structure in Central Asia and Tibetan Plateau by seismic reflection profiles, attenuation tomography, surface wave tomography, and body-wave travel time tomography.



Lian-Feng Zhao is a professor at the Institute of Geology and Geophysics, Chinese Academy of Sciences. His research interest focuses on conducting seismic attenuation tomography to explore the crust and upper mantle structure and understand the dynamics and evolution of the lithosphere. He also has a keen interest in researching source mechanism and seismological characteristics of unconventional earthquakes such as nuclear explosions.



Liang Zhao is a professor at the Institute of Geology and Geophysics, Chinese Academy of Sciences. The primary goal of his research is directed toward understanding the structure, dynamics, and evolution of the Earth's interior by waveform modeling, receiver function, shear wave splitting and tomography. He also has a strong interest in developing new methodologies for simulating seismic wave propagation through the heterogeneous and anisotropic media.